

## 2次元ファラデー波における1:3共鳴

京大・情報学研究科 芳松 克則 (Katsunori YOSHIMATSU)  
京大・情報学研究科 船越 満明 (Mitsuaki FUNAKOSHI)

### Abstract

Third-harmonic resonance of capillary-gravity waves in two-dimensional Faraday waves due to the parametric excitation of the lower-frequency mode is examined for infinite depth. The amplitude equation incorporating both a small detuning from this internal resonance and that from the external resonance with the vertical oscillation of a container is derived using the method of reductive perturbation and also including a linear damping. This equation has mixed-wave solutions: periodic and chaotic solutions as well as stationary solutions. Moreover, we find two more hysteresis regions of stationary solutions, in addition to the hysteresis region observed also for a single-mode Faraday wave. Some periodic solutions become chaotic through a series of period-doubling bifurcations.

## 1 Introduction

Breakdown of the ordinary weakly nonlinear expansion for deep capillary-gravity waves occurs at certain discrete wavenumbers  $\hat{k}_n = [\rho g / (n\sigma)]^{1/2}$  ( $n = 2, 3, \dots$ ). [1] Here,  $g$ ,  $\sigma$  and  $\rho$  are the gravitational acceleration, the surface tension coefficient and the density of a fluid, respectively. This breakdown is caused by the resonance between the fundamental wave of wavenumber  $\hat{k}_n$  and its  $n$ -th harmonic, called the  $n$ -th harmonic resonance. Among this type of resonances, the third-harmonic resonance, of  $n = 3$ , happens between a wave of frequency  $52.6 \text{ s}^{-1}$  and wavenumber  $2.12 \text{ cm}^{-1}$  and its third harmonic for surface waves of deep, clean water ( $\sigma = 73 \text{ dyn/cm}$ ,  $\rho = 1.00 \text{ g/cm}^3$ ). The third-harmonic resonance of weakly nonlinear travelling waves was investigated both theoretically and experimentally by McGoldrick [2] and examined theoretically by Nayfeh. [3, 4] However, as far as we know, there is no study on the third-harmonic resonance of nonlinear standing waves under no forcing and damping.

Faraday waves are widely known as standing waves subharmonically excited by the forcing of the vertical oscillation of the container of a fluid. Weakly nonlinear behavior of Faraday waves was theoretically studied by Miles [5] for gravity waves. He showed that when the forcing amplitude exceeds a threshold value determined by a damping coefficient and a detuning from the exact resonance, the quiescent state of the fluid becomes unstable and a standing wave is excited. He also found a hysteresis phenomenon of the excited standing wave when half of the forcing frequency is slightly smaller than the frequency of this wave.

In the present paper, the third-harmonic resonance in two-dimensional Faraday waves is examined in which the fundamental wave is subharmonically excited. In § 2, we derive nonlinear equation for the amplitudes of the fundamental mode and its third harmonic of capillary-gravity waves in a deep fluid. In this equation, both small detunings from internal and external resonances as well as a small

linear damping are included. In § 3, the results on the properties of the stationary solutions of this equation and the hysteresis phenomena of these solutions are shown. Also, the chaotic solutions generated by a series of the period-doubling bifurcations are shown in this section. Finally, conclusions are given in § 4.

## 2 Amplitude Equation with Third-Harmonic Resonance

For linear capillary-gravity surface waves in a deep fluid, their wavenumbers  $k_i$  and frequencies  $\bar{\omega}_i$  satisfy the dispersion relation

$$\bar{\omega}_i^2 = k_i g (1 + \Gamma_i), \quad (1)$$

with  $\Gamma_i = \sigma k_i^2 / (\rho g)$ . Here,  $g$ ,  $\sigma$  and  $\rho$  are the gravitational acceleration, the surface tension coefficient and the density of the fluid, respectively. The third-harmonic resonance incorporating a small detuning between a fundamental wave ( $i = 1$ ) and its third harmonic ( $i = 3$ ) occurs when the relations

$$k_3 = 3k_1, \quad \bar{\omega}_3 = 3\bar{\omega}_1 + \hat{\omega}, \quad (2)$$

are satisfied. Here  $\hat{\omega}$  implies a small detuning from the exact third-harmonic resonance. For these waves,  $\Gamma_1$  and  $\Gamma_3$  have slight discrepancies from  $1/3$  and  $3$ , respectively. Furthermore, the nondimensional frequencies  $\omega_i$  ( $i = 1, 3$ ) of these waves defined by  $\omega_i = \bar{\omega}_i / \sqrt{gk_1}$  are close to  $2/\sqrt{3}$  and  $2\sqrt{3}$ , respectively. In the following part of the present paper, all variables are nondimensionalized using the length  $1/k_1$  and the time  $1/\sqrt{gk_1}$ .

The vertical sinusoidal oscillation of a container with a dimensionless acceleration  $f \cos(2\Omega t)$  can generate the standing wave of dimensionless frequency  $\Omega$ . Here  $t$  is the dimensionless time. This subharmonically excited wave is called Faraday wave. In the present paper, we consider the combination of the third-harmonic resonance and the subharmonic excitation of the fundamental wave by assuming that forcing frequency  $2\Omega$  is close to  $2\omega_1$ .

In the derivation of the amplitude equation for the two resonant waves, we assume the two-dimensional irrotational flow of an incompressible inviscid fluid. Dimensionless free-surface displacement and velocity potential are denoted by  $z = \eta(x, t)$  and  $\phi(x, z, t)$ , respectively. Here  $x$  and  $z$  are dimensionless horizontal and upward vertical coordinates fixed to the container. We also assume that the depth of the fluid is large enough to use the approximation of infinite depth.

The continuity equation is written as Laplace's equation

$$\nabla^2 \phi = 0 \quad \text{for} \quad -\infty < z \leq \eta, \quad (3)$$

where  $\nabla = (\partial_x, \partial_z)$ . From Bernoulli's theorem, the dynamical condition at the free surface is

$$\partial_t \phi + \frac{1}{2} (\nabla \phi)^2 + [1 + f \cos(2\Omega t)] \eta - \Gamma_1 \partial_x^2 \eta \left[ 1 + (\partial_x \eta)^2 \right]^{-3/2} = 0 \quad \text{at} \quad z = \eta. \quad (4)$$

The kinematical condition at the free surface is

$$\partial_t \eta + \partial_x \phi \partial_x \eta = \partial_z \phi \quad \text{at} \quad z = \eta. \quad (5)$$

Furthermore, the boundary condition

$$\nabla\phi \rightarrow \mathbf{0} \quad \text{as } z \rightarrow -\infty, \quad (6)$$

should be satisfied.

Expanding eqs.(4) and (5) around  $z = 0$ , we obtain

$$\begin{aligned} & \partial_t\phi - \Gamma_1\partial_x^2\eta + [1 + f\cos(2\Omega t)]\eta + \eta\partial_z\partial_t\phi \\ & + \frac{1}{2}\eta^2\partial_z^2\partial_t\phi + \frac{1}{2}(\nabla\phi)^2 + \frac{1}{2}\eta\partial_z(\nabla\phi)^2 + \frac{3}{2}\Gamma_1\partial_x^2\eta(\partial_x\eta)^2 = 0 \quad \text{at } z = 0, \end{aligned} \quad (7)$$

$$\partial_t\eta - \partial_z\phi + \partial_x\eta\partial_x\phi + \eta\partial_x\eta\partial_z\partial_x\phi - \eta\partial_z^2\phi - \frac{1}{2}\eta^2\partial_z^3\phi = 0 \quad \text{at } z = 0, \quad (8)$$

after neglecting the terms of the fourth or higher order with respect to  $\eta$  and  $\phi$ . Next, we introduce the expanded forms of  $\phi$  and  $\eta$  with respect to  $\epsilon$  expressed as

$$\phi = \epsilon\phi_1 + \epsilon^2\phi_2 + \epsilon^3\phi_3 + \dots, \quad \eta = \epsilon\eta_1 + \epsilon^2\eta_2 + \epsilon^3\eta_3 + \dots, \quad (9)$$

where  $\epsilon (\ll 1)$  is a parameter representing wave steepness. Moreover, we assume that the relation

$$\Gamma_1 = \frac{1}{3} + \epsilon^2\gamma_1, \quad (10)$$

is satisfied. The term  $\epsilon^2\gamma_1$  in eq.(10) represents a small detuning from the exact third-harmonic resonance, because the dimensionless discrepancy  $\hat{\omega}/\sqrt{gk_1}$  from the exact resonance is expressed by  $3\sqrt{3}\epsilon^2\gamma_1/2$  in the leading order. Furthermore, assuming that  $f = O(\epsilon^2)$  and  $\Omega - \omega_1 = O(\epsilon^2)$ , we write as

$$f = \epsilon^2F, \quad (11)$$

$$\Omega = \omega_1 + \epsilon^2\delta_1. \quad (12)$$

Therefore,  $\delta_1$  expresses a small mismatch from the exact external resonance. Moreover, a slow time variable  $\tau = \epsilon^2t$  is introduced.

Substituting eqs.(9) and (10) into the Taylor expansion of eqs.(7) and (8) around  $z = 0$ , and using eq.(11) and the replacement  $\partial_t \rightarrow \partial_t + \epsilon^2\partial_\tau$ , we obtain the following equations in  $O(\epsilon)$ :

$$\partial_t\phi_1 - \frac{1}{3}\partial_x^2\eta_1 + \eta_1 = 0 \quad \text{at } z = 0, \quad (13)$$

$$\partial_t\eta_1 - \partial_z\phi_1 = 0 \quad \text{at } z = 0. \quad (14)$$

The equations obtained in  $O(\epsilon^2)$  and  $O(\epsilon^3)$  are shown in Appendix A as eqs.(22)–(25).

Since we consider the waves composed of the fundamental mode and its third harmonic, we assume that  $\eta_1$  and  $\phi_1$  are written as

$$\eta_1 = a(\tau)\exp(-i\omega t)\cos x + b(\tau)\exp(-3i\omega t)\cos 3x + \text{c.c.}, \quad (15)$$

$$\begin{aligned} \phi_1 &= -i\omega a(\tau)\exp(z)\exp(-i\omega t)\cos x \\ &\quad -i\omega b(\tau)\exp(3z)\exp(-3i\omega t)\cos 3x + \text{c.c.}, \end{aligned} \quad (16)$$

where  $\omega = 2/\sqrt{3}$  is the value of  $\omega_1$  in the leading order, and c.c. denotes the complex conjugate of the preceding terms. Also  $a(\tau)$  and  $b(\tau)$  express the complex

amplitudes of the fundamental wave and its third harmonic, respectively. Using eqs.(3), (6), (9), (12), (13), (14), (22)–(25), we obtain in  $O(\epsilon^2)$  the expressions of  $(\eta_2, \phi_2)$  given in Appendix B as eqs.(26) and (27). Furthermore, in  $O(\epsilon^3)$ , the following equation for  $a$  and  $b$  is derived from solvability conditions:

$$\begin{aligned} \frac{da}{d\tau} = & -i\frac{\gamma_1}{2\omega}a - i\frac{F}{4\omega}a^* \exp(-2i\Delta\tau) \\ & -i\omega\frac{369}{64}b(a^*)^2 - i\omega\frac{145}{448}|a|^2a + i\omega\frac{243}{400}|b|^2a, \end{aligned} \quad (17)$$

$$\frac{db}{d\tau} = -i\frac{9\gamma_1}{2\omega}b - i\omega\frac{123}{64}a^3 + i\omega\frac{115209}{4160}|b|^2b + i\omega\frac{243}{400}|a|^2b, \quad (18)$$

where  $*$  denotes the complex conjugate, and  $\Delta = \delta_1 + \gamma_1/(2\omega)$  represents the small discrepancy between  $\Omega$  and  $\omega$ , because of eq.(12) and the relation  $(\omega_1 - \omega)/\epsilon^2 = \gamma_1/(2\omega) + O(\epsilon)$  obtained from eqs.(1) and (10).

Here, we introduce the linear damping of dimensionless coefficients  $\alpha_1$  and  $\alpha_3$  for the fundamental wave and its third harmonic, respectively. If we consider the situation in which the contribution of the damping within the boundary layers on the sidewalls of the container to the total damping is dominant and other damping due to the bulk flow, surface contamination and capillary hysteresis can be neglected, the damping coefficient is proportional to the square root of wave frequency.[6, 7] Therefore, we assume the relation  $\alpha_3 = \sqrt{3}\alpha_1$ .

If we replace the variables  $a \exp(i\Delta\tau)/(2\sqrt{\alpha_1/\omega})$ ,  $3b \exp(3i\Delta\tau)/(2\sqrt{\alpha_1/\omega})$ ,  $\alpha_1\tau$ ,  $F/(4\alpha_1\omega)$ ,  $\delta_1/\alpha_1$  and  $\gamma_1/(2\alpha_1\omega)$  by  $A$ ,  $B$ ,  $T$ ,  $\beta$ ,  $\delta$  and  $\gamma$ , respectively, eqs.(17) and (18) with the inclusion of the above linear damping is rewritten as

$$\frac{dA}{dT} = -A + i\delta A - i\beta A^* - i\frac{123}{16}B(A^*)^2 - i\frac{145}{112}|A|^2A + i\frac{27}{100}|B|^2A, \quad (19)$$

$$\frac{dB}{dT} = -\sqrt{3}B + i(3\delta - 6\gamma)B - i\frac{369}{16}A^3 + i\frac{12801}{1040}|B|^2B + i\frac{243}{100}|A|^2B. \quad (20)$$

### 3 Solutions of Amplitude Equation

In this section, the results on the solutions of eqs.(19) and (20) for several values of  $(\delta, \gamma, \beta)$  are shown. Furthermore, the solutions are examined in detail for the special cases of exact internal resonance ( $\gamma = 0$ ), exact external resonance ( $\delta = 0$ ) and of  $\gamma = \pm\delta$ . As in the case of a single-mode Faraday wave,[5] the null solution of eqs.(19) and (20) is linearly stable when  $\beta \leq \beta_c$  and unstable when  $\beta > \beta_c$ , where  $\beta_c = (1 + \delta^2)^{1/2}$ . Moreover, only the mixed-wave solutions can be expected since eqs.(19) and (20) has no pure-wave solution.

#### 3.1 Stationary mixed-wave solutions

If we assume that  $dA/dT = 0$  and  $dB/dT = 0$  in eqs.(19) and (20), we obtain the relation

$$\begin{aligned} A^2 = & -\frac{i}{\beta} \left( \frac{\sqrt{3}}{3}|B|^2 + |A|^2 \right) \\ & + \frac{1}{\beta} \left[ \delta(|A|^2 - |B|^2) + 2\gamma|B|^2 - \frac{145}{112}|A|^4 - \frac{4267}{1040}|B|^4 - \frac{81}{50}|A|^2|B|^2 \right], \end{aligned} \quad (21)$$

from this equation. Taking the square of the modulus of eq.(21), we find that the stationary mixed-wave solution exists only for  $\beta > 1$ . Furthermore, the sign of  $\text{Re}A$  of this solution is always opposite to that of  $\text{Im}A$  because  $\text{Im}(A^2)$  is negative from eq.(21). This characteristic is the same as that of the solution for a single-mode Faraday wave. Stationary mixed-wave solutions appear through the pitchfork bifurcation from the null solution at  $\beta = \beta_c$  for all  $(\delta, \gamma)$ . As shown in Appendix C, this bifurcation is supercritical (subcritical) when  $\delta < 0$  ( $\delta > 0$ ). This sign of  $\delta$  for each bifurcation is opposite to that obtained by Miles[5] for a single-mode Faraday wave. This is because the sign of the coefficient of nonlinear term  $|A|^2 A$  of eq.(19) for capillary-gravity waves with  $\Gamma_1 \approx 1/3$  is different from that for gravity waves examined by him. The stationary mixed-wave solutions of eqs.(19) and (20) were also examined numerically using the Brent method. Figure 1 shows the regions of the existence of the mixed-wave solutions and their stability on the  $(\delta, \beta)$  or  $(\gamma, \beta)$  plane. Within the region of  $\beta > \beta_c$  or regions  $H_1$  and  $H_2$  in this figure, there is at least one stable stationary mixed-wave solution except for region  $U$  shown in Figs. 1(a), 1(b) and 1(c). In regions  $H_1$ ,  $H_2$  and  $H_3$ , we find the hysteresis phenomena of this solution, as will be shown in detail in the following part of this subsection. No stable stationary solution exists in region  $U$ , at the boundary of which the stable stationary solutions become unstable by the Hopf bifurcations. Examples of the dependence of the stationary mixed-wave solutions on  $\beta$  are given in Fig. 2 for a few pairs of  $(\delta, \gamma)$ . Although the mixed-wave solutions are obtained as a pair with different signs, only the solutions with  $\text{Re}A > 0$  are shown in this figure.

The solutions for  $\gamma = 0$  (shown in Fig. 1(a)) and for  $\gamma = -\delta$  (shown in Fig. 1(c)) have similar characteristics. In region  $H_1$  of these figures, the solution subcritically bifurcating from the null solution at  $\beta = \beta_c$  gives the hysteresis behavior. As illustrated in Fig. 2(a), the branch of this solution is folded once at the lower boundary of region  $H_1$ , and its stability changes at the point of the saddle-node bifurcation. Although region  $H_1$  exists for all positive  $\delta$ , its width in the  $\beta$  direction decreases to zero as  $\delta$  tends to zero. If  $-0.994 \leq \delta < 0$  for  $\gamma = 0$  or if  $-0.580 \leq \delta < 0$  for  $\gamma = -\delta$ , no hysteresis region of the stationary solutions is found. This is because the branch of the solution supercritically bifurcating from the null solution at  $\beta = \beta_c$  extends to large  $\beta$  monotonically, as illustrated in Fig. 2(b). When  $\delta < -0.994$  in Fig. 1(a) or  $\delta < -0.580$  in Fig. 1(c), we find another hysteresis region  $H_2$ . As illustrated in Fig. 2(c), the branch of the solution supercritically bifurcating at  $\beta = \beta_c$  is folded twice before it finally reaches sufficiently large  $\beta$ . The  $\beta$ 's of the first and second saddle-node bifurcations of the solutions on this branch give the upper and lower boundaries of region  $H_2$ , where the stability of the solution changes. This upper boundary is just above  $\beta = \beta_c$  both for  $\gamma = 0$  and for  $\gamma = -\delta$ .

If exact external resonance ( $\delta = 0$ ) is assumed, no hysteresis region is observed, as shown in Fig. 1(b). The branch of the solution bifurcating from the null solution at  $\beta = 1$  extends to large  $\beta$  monotonically, similarly to the solution shown in Fig. 2(b). Next, for  $\gamma = \delta$ , we find hysteresis region  $H_3$  in addition to region  $H_1$ , as shown in Fig. 1(d). Although the width of region  $H_1$  is too narrow to be recognized in this figure, this region exists just below the curve of  $\beta = \beta_c$  for all positive  $\delta$ . As illustrated in Fig. 2(d), the branch of the solution subcritically bifurcating at  $\beta = \beta_c$  is folded three times, which results in the change of its stability at each point of the saddle-node bifurcations. The  $\beta$ 's of the second and third foldings

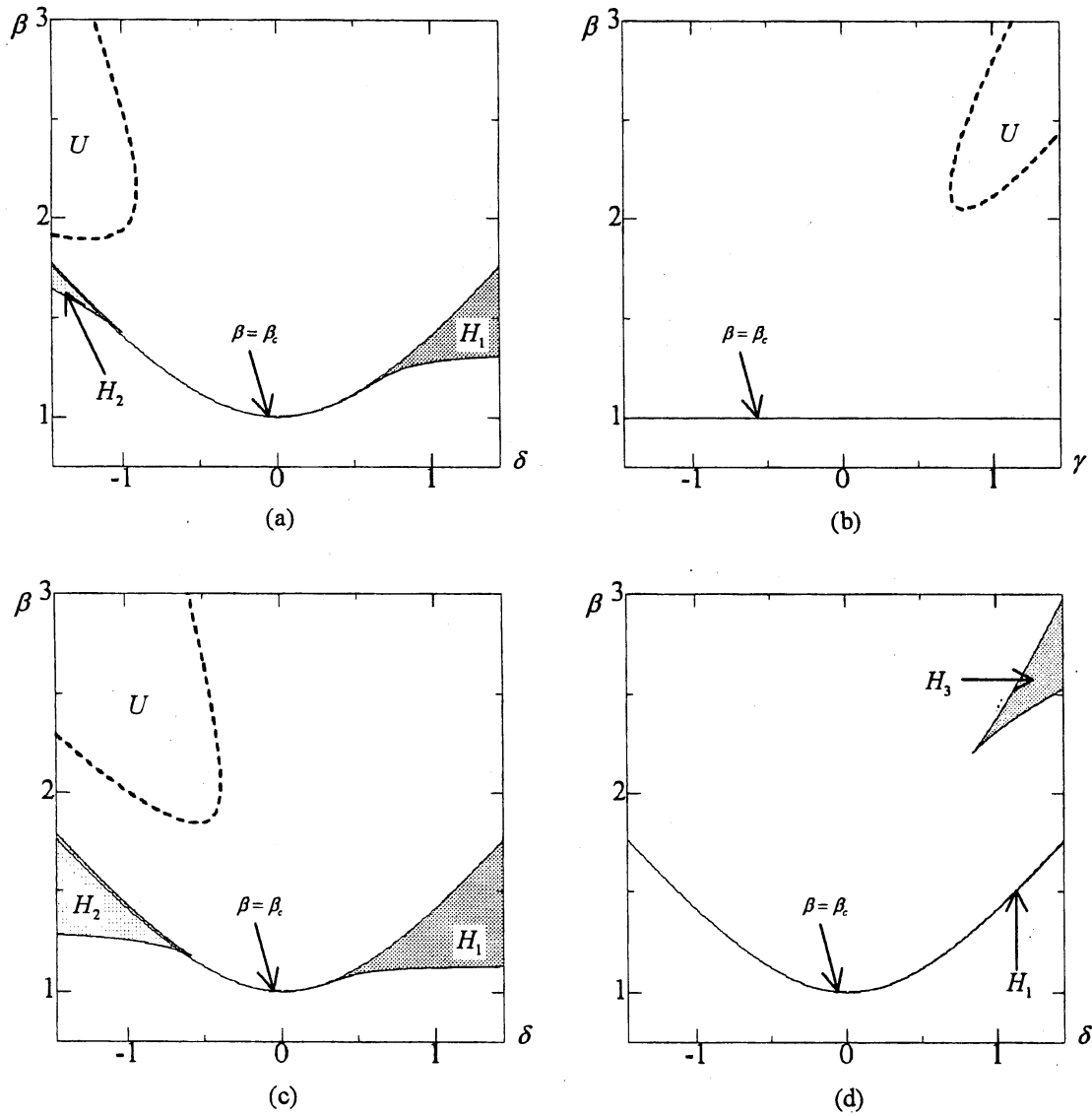


Figure 1: Regions of the existence of the stationary mixed-wave solutions on the  $(\delta, \beta)$  or  $(\gamma, \beta)$  plane. (a)  $\gamma = 0$ , (b)  $\delta = 0$ , (c)  $\gamma = -\delta$ , (d)  $\gamma = \delta$ . Regions denoted by  $H_1$ ,  $H_2$  and  $H_3$  are hysteresis regions. There is no stable stationary solution in region  $U$ .

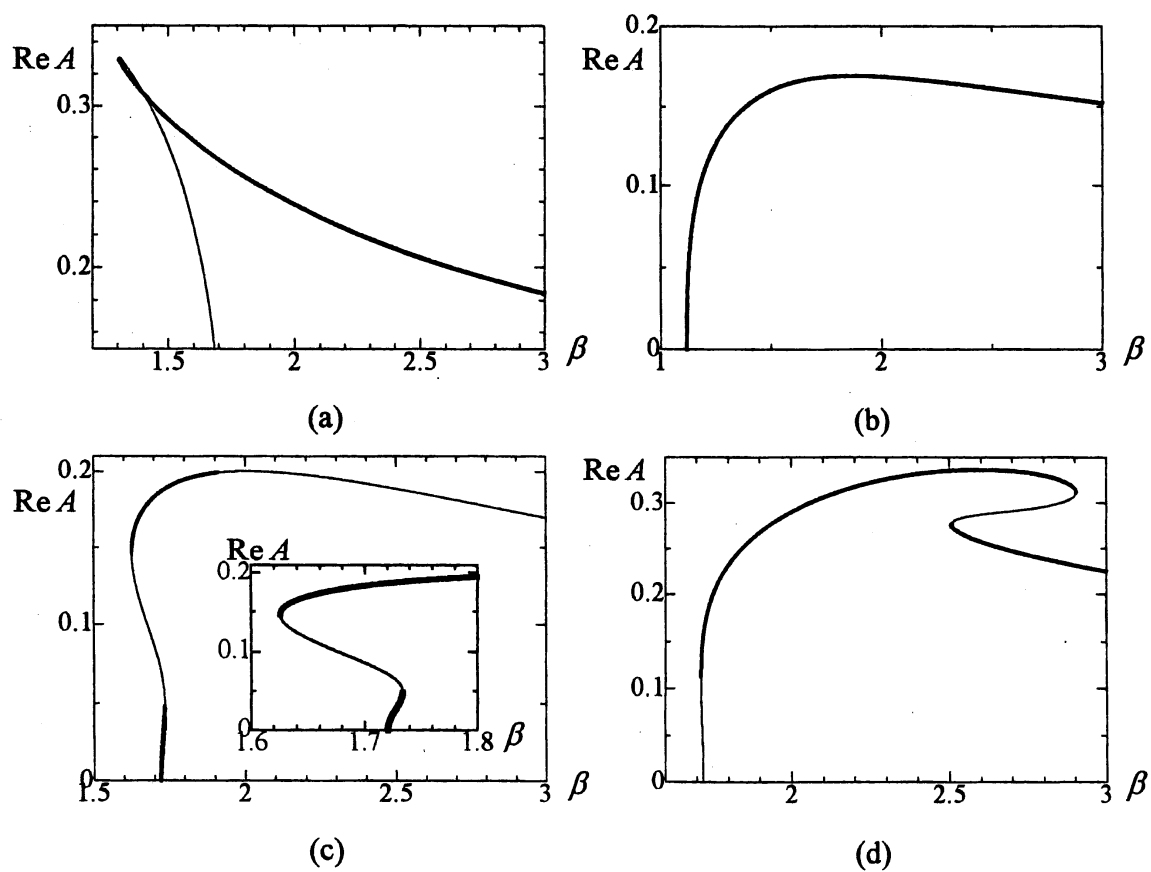


Figure 2: Examples of the dependence of the stationary mixed-wave solutions on  $\beta$ . (a)  $(\delta, \gamma) = (1.4, 0)$ , (b)  $(\delta, \gamma) = (-0.5, 0)$ , (c)  $(\delta, \gamma) = (-1.4, 0)$ , and (d)  $(\delta, \gamma) = (1.4, 1.4)$ . Only the values of  $\text{Re}A$  are shown. The magnification of  $\text{Re}A$  around  $\beta = \beta_c$  is also in (c). Thick and thin curves denote stable and unstable solutions, respectively.

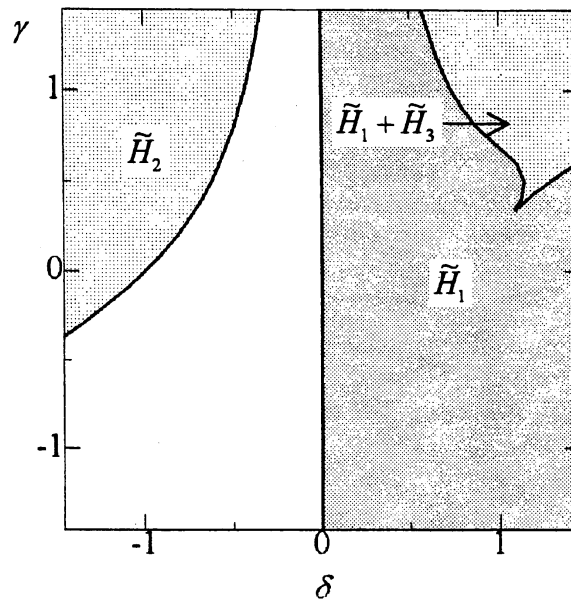


Figure 3: Regions  $\tilde{H}_i$  ( $i = 1, 2, 3$ ) on the  $(\delta, \gamma)$  plane within which hysteresis regions  $H_i$  are found.

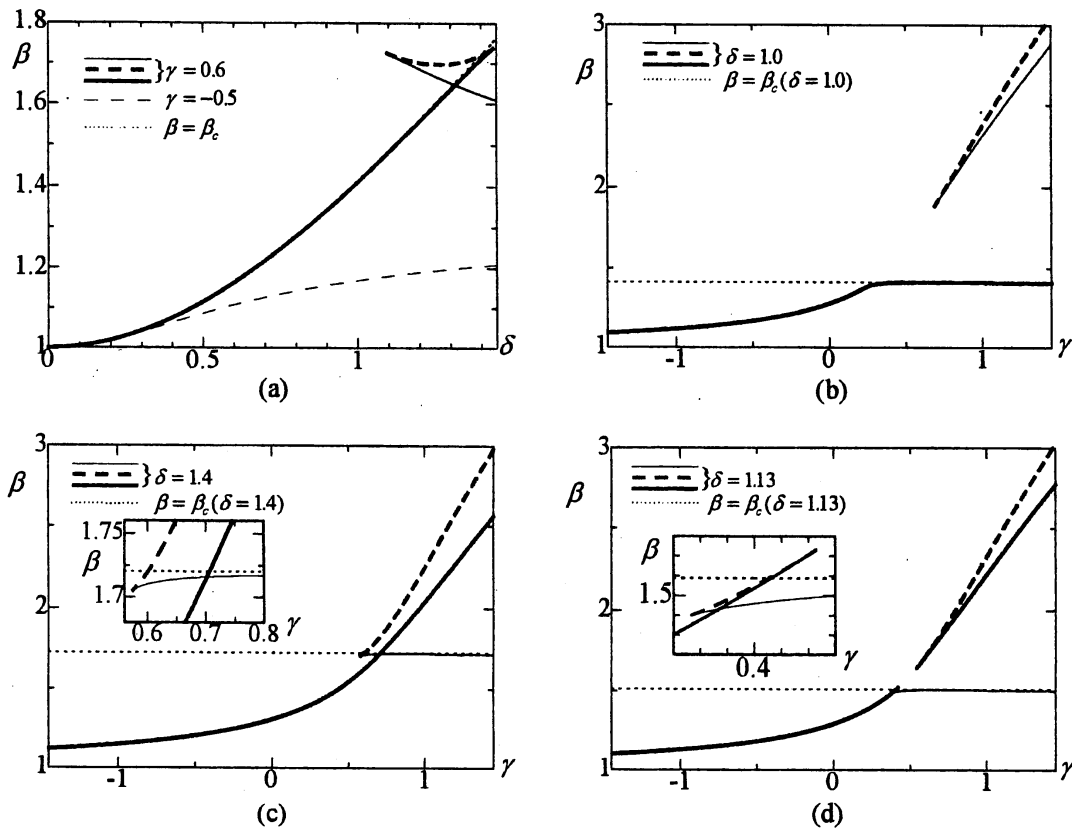


Figure 4: Examples of the saddle-node bifurcation points on the  $(\delta, \beta)$  or  $(\gamma, \beta)$  plane.

correspond to the upper and lower boundaries of region  $H_3$ .

Figure 3 shows regions  $\tilde{H}_1$ ,  $\tilde{H}_2$  and  $\tilde{H}_3$  on the  $(\delta, \gamma)$  plane within which hysteresis regions  $H_1$ ,  $H_2$  and  $H_3$  are found, respectively. Since the bifurcation at  $\beta = \beta_c$  is subcritical when  $\delta > 0$ , region  $\tilde{H}_1$  covers all the half plane  $\delta > 0$ . Moreover, hysteresis region  $H_3$  also exists in the region denoted by  $\tilde{H}_1 + \tilde{H}_3$ . On the other hand, if  $\delta \leq 0$ , no hysteresis phenomenon is observed in the white region of this figure, and only hysteresis region  $H_2$  exists in region  $\tilde{H}_2$ . As  $|\delta|$  decreases, region  $H_2$  always terminates as a cusp, as shown in Figs. 1(a) and 1(c), and this cusp point corresponds to the boundary of region  $\tilde{H}_2$  in Fig. 3.

Since the bifurcations in the region of  $\delta > 0$  in Fig. 3 can be a little complicated, these bifurcations are explained by showing in Fig. 4 the bifurcation points on the  $(\delta, \beta)$  or  $(\gamma, \beta)$  plane for a few fixed values of  $\gamma$  or  $\delta$ . If  $\gamma$  is fixed to a value sufficiently smaller than the lower end of region  $\tilde{H}_1 + \tilde{H}_3$  of Fig. 3, the width of region  $H_1$  in the  $\beta$  direction increases rapidly with increasing  $\delta$ , as illustrated for  $\gamma = -0.5$  in Fig. 4(a). However, if we choose a larger fixed value of  $\gamma$  above this lower end, this width is small up to a relatively large value of  $\delta$ . An example is shown in Fig. 4(a) for  $\gamma = 0.6$ . For this  $\gamma$ , if  $0 < \delta < 1.439$ , since the curve of  $\beta = \beta_c$  is just above a thick solid curve expressing the saddle-node bifurcation point corresponding to the lower boundary of region  $H_1$ , the width of region  $H_1$  is quite small. However, at  $\delta = 1.095$ , a pair of the saddle-node bifurcations expressed by thin solid and thick dashed curves appear on the branch of the solutions, on the opposite side to the bifurcation point of  $\beta = \beta_c$  from the existing saddle-node bifurcation point. This appearance yields region  $H_3$ . With increasing  $\delta$ , the saddle-node bifurcation points denoted by the thick dashed and thick solid curves coalesce and disappear at  $\delta = 1.439$ . Therefore, at this  $\delta$ , region  $H_3$  vanishes and region  $H_1$  expands abruptly due to the change of its lower boundary from the thick solid curve to the thin solid curve.

Next, if  $\delta$  is fixed to a positive value which is on the left of the cusp point at the lower boundary of region  $\tilde{H}_1 + \tilde{H}_3$  of Fig. 3 and inside it, as  $\gamma$  increases, the width of region  $H_1$  in the  $\beta$  direction first decreases and then keeps small for large  $\gamma$ , as illustrated for  $\delta = 1.0$  in Fig. 4(b). Moreover, a pair of the saddle-node bifurcations appear at  $\gamma = 0.686$ . These bifurcations generate hysteresis region  $H_3$  surrounded by thick dashed and thin solid curves for  $\gamma > 0.686$ . However, for a larger fixed  $\delta$  which is within region  $\tilde{H}_1 + \tilde{H}_3$  for sufficiently large  $\gamma$ , the abrupt change in the width of region  $H_1$  is observed. An example is shown for  $\delta = 1.4$  in Fig. 4(c), in which a thick solid curve gives the lower boundary of region  $H_1$  if  $\gamma < 0.574$ . However, at  $\gamma = 0.574$ , a pair of the saddle-node bifurcations denoted by thick dashed and thin solid curves appear on the branch of the solution, between the existing saddle-node bifurcation point and the bifurcation point of  $\beta = \beta_c$ . This causes the abrupt decrease in the width of region  $H_1$  because the lower boundary of this region changes to the thin solid curve at this  $\gamma$ . Furthermore, the appearance of these bifurcations yields region  $H_3$  delimited by the thick dashed and thick solid curves. For  $\gamma > 0.574$ , as  $\gamma$  increases, region  $H_3$  shifts to larger  $\beta$  and its width increases, whereas the width of region  $H_1$  first decreases and then increases gradually. A little different behavior of bifurcation points is observed for  $\delta = 1.13$ . That is, as shown in Fig. 4(d), with increasing  $\gamma$ , after the appearance of the saddle-node bifurcation points expressed by thick dashed and thin solid curves at  $\gamma = 0.377$ , the saddle-node bifurcation points denoted by thick dashed and thick

solid curves coalesce and vanish at  $\gamma = 0.423$ , which results in the disappearance of region  $H_3$ . However, a pair of the saddle-node bifurcations appear again at  $\gamma = 0.544$ , and region  $H_3$  bounded by thick dashed and thick solid curves is observed again for  $\gamma > 0.544$ . This non-existence of region  $H_3$  for  $0.423 < \gamma < 0.544$  corresponds to the concave part of region  $\tilde{H}_1 + \tilde{H}_3$  near its lower end in Fig. 3.

In Faraday waves without the third-harmonic resonance, that is, in eq.(19) without the terms  $B(A^*)^2$  and  $|B|^2 A$ , we obtain the hysteresis region of the stationary solutions surrounded by  $\beta = \beta_c$  and  $\beta = 1$  for  $\delta > 0$ . Although hysteresis region  $H_1$  in the present study corresponds to this hysteresis region, region  $H_1$  is smaller than this region irrespective of the value of  $\gamma$ , because the stationary mixed-wave solutions are possible only for  $\beta > 1$ , as was shown in the beginning of this subsection. Furthermore, no other hysteresis region is found for this case. Therefore, one of the characteristics of Faraday waves with the third harmonic resonance in comparison with a single-mode Faraday wave is the existence of two additional hysteresis regions  $H_2$  and  $H_3$  for  $(\delta, \gamma)$  within regions  $\tilde{H}_2$  and  $\tilde{H}_3$ .

### 3.2 Non-stationary mixed-wave solutions

In this subsection, the results on the non-stationary mixed-wave solutions of eqs.(19) and (20) are given. We numerically computed the solutions of eqs.(19) and (20) using the Adams method. After discarding initial transients, the solutions are expressed by the set composed of the values of  $\text{Re}B$  when the orbit of the solution intersects a hyperplane  $\text{Re}A = \langle \text{Re}A \rangle$  in the decreasing direction of  $\text{Re}A$ . Here  $\langle \text{Re}A \rangle$  is the average value of  $\text{Re}A$  on each attractor. This set is composed of only a few points for limit cycles, whereas it is composed of many points for chaotic attractors. The variations of the solutions with slow increase in  $\beta$  are shown in Fig. 5 for a values of  $(\delta, \gamma) = (-1.2, 0.7)$ . We can observe the appearance of chaotic solutions through a series of the period-doubling bifurcations and their return to the simple periodic solutions through a series of the reversed period-doubling bifurcations in Fig. 5.

## 4 Conclusions

Third-harmonic resonance of capillary-gravity waves in two-dimensional Faraday waves due to the parametric excitation of the lower-frequency mode is examined for infinite depth. We derive amplitude equations (19) and (20) which includes both a small detuning from this internal resonance and that from the external resonance with the vertical oscillation of a container and also a linear damping, using the method of reductive perturbation.

We obtain a few kinds of mixed-wave solutions of this equation: periodic and chaotic solutions as well as stationary solutions. Moreover, we find two more hysteresis regions  $H_2$  and  $H_3$  of stationary solutions, in addition to hysteresis region  $H_1$  observed also for a single-mode Faraday wave. Region  $H_1$  is smaller than that obtained for a single-mode Faraday wave, irrespective of the value of the detuning from the exact internal resonance.

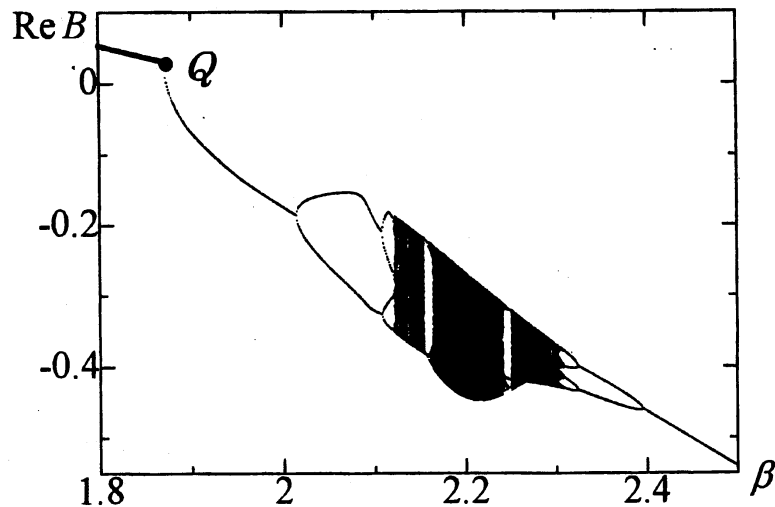


Figure 5: Variations of non-stationary solutions of eqs.(19) and (20) with slow increase in  $\beta$  for  $(\delta, \gamma) = (-1.2, 0.7)$ . The increment of  $\beta$  is 0.001, and the data for  $1500 \leq T \leq 2000$  are used in drawing this figure. These solutions are expressed by showing the values of  $\text{Re}B$  when the conditions  $\text{Re}A = \langle \text{Re}A \rangle$  and  $\text{Re}(dA/dT) < 0$  are satisfied. Here  $\langle \text{Re}A \rangle$  is the average value of  $\text{Re}A$  on each periodic orbit. Thick solid curve denotes the values of  $\text{Re}B$  of the stable stationary solutions.  $Q$  is the Hopf bifurcation point of the stationary solution. This bifurcation occurs at  $\beta = 1.872$ .

## Acknowledgements

The authors would like to thank Professor A. D. D. Craik and Associated Professor Y. Murakami for valuable discussions on Faraday waves.

## A Equations in $O(\epsilon^2)$ and $O(\epsilon^3)$

In  $O(\epsilon^2)$ , we obtain

$$\partial_t \phi_2 - \frac{1}{3} \partial_x^2 \eta_2 + \eta_2 + \eta_1 \partial_z \partial_t \phi_1 + \frac{1}{2} (\nabla \phi_1)^2 = 0 \quad \text{at } z = 0, \quad (22)$$

$$\partial_t \eta_2 - \partial_z \phi_2 + \partial_x \phi_1 \partial_x \eta_1 - \eta_1 \partial_z^2 \phi_1 = 0 \quad \text{at } z = 0. \quad (23)$$

Furthermore, the following equations are derived in  $O(\epsilon^3)$ :

$$\begin{aligned} & \partial_t \phi_3 + \partial_\tau \phi_1 - \frac{1}{3} \partial_x^2 \eta_3 - \gamma_1 \partial_x^2 \eta_1 + \eta_3 + F \cos(2\Omega t) \eta_1 \\ & + \frac{1}{2} \partial_x^2 \eta_1 (\partial_x \eta_1)^2 + \eta_2 \partial_z \partial_t \phi_1 + \eta_1 \partial_z \partial_t \phi_2 \\ & + \frac{1}{2} \eta_1^2 \partial_z^2 \partial_t \phi_1 + \nabla \phi_2 \cdot \nabla \phi_1 + \frac{1}{2} \eta_1 \partial_z (\nabla \phi_1)^2 = 0 \quad \text{at } z = 0, \end{aligned} \quad (24)$$

$$\begin{aligned} & \partial_t \eta_3 + \partial_\tau \eta_1 - \partial_z \phi_3 - \eta_2 \partial_z^2 \phi_1 - \eta_1 \partial_z^2 \phi_2 \\ & - \frac{1}{2} \eta_1^2 \partial_z^3 \phi_1 + \partial_x \phi_1 \partial_x \eta_2 + \partial_x \phi_2 \partial_x \eta_1 + \eta_1 \partial_x \eta_1 \partial_z \partial_x \phi_1 = 0 \quad \text{at } z = 0. \end{aligned} \quad (25)$$

## B Expressions of $\eta_2$ and $\phi_2$

$$\begin{aligned}\eta_2 = & 2a^2 \exp(-2i\omega t) \cos(2x) - \frac{6}{5}b^2 \exp(-6i\omega t) \cos(6x) \\ & - 4ab \exp(-4i\omega t) \cos(4x) - \frac{8}{25}ab \exp(-4i\omega t) \cos(2x) \\ & + 8a^*b \exp(-2i\omega t) \cos(2x) + \frac{4}{5}a^*b \exp(-2i\omega t) \cos(4x) \\ & + \frac{2}{7}|a|^2 \cos(2x) + \frac{6}{13}|b|^2 \cos(6x) + \text{c.c.}\end{aligned}\quad (26)$$

$$\begin{aligned}\phi_2 = & -\frac{3}{2}i\omega a^2 \exp(2z) \exp(-2i\omega t) \cos(2x) + i\frac{27}{10}\omega b^2 \exp(6z) \exp(-6i\omega t) \cos(6x) \\ & + 6i\omega ab \exp(4z) \exp(-4i\omega t) \cos(4x) + \frac{57}{25}i\omega ab \exp(2z) \exp(-4i\omega t) \cos(2x) \\ & - 6i\omega a^*b \exp(2z) \exp(-2i\omega t) \cos(2x) + \frac{3}{5}i\omega a^*b \exp(4z) \exp(-2i\omega t) \cos(4x) \\ & + \frac{1}{2}i\omega a^2 \exp(-2i\omega t) + \frac{3}{2}i\omega b^2 \exp(-6i\omega t) + \text{c.c.}\end{aligned}\quad (27)$$

## C Bifurcation at $\beta = \beta_c$

From eqs.(19) and (20), we find that for sufficiently small stationary solutions bifurcating from  $(A, B) = (0, 0)$  at  $\beta = \beta_c$ ,  $|B|$  should be  $O(|A|^3)$  and the following relations should be satisfied:

$$B = c_1 \frac{3\delta - 6\gamma - i\sqrt{3}}{1 + 3(\delta - 2\gamma)^2} A^3 + O(|A|^5), \quad (28)$$

$$-A + i\delta A - i\beta A^* - ic_2 |A|^2 A - (p_1 + ip_2) |A|^4 A = O(|A|^7), \quad (29)$$

where  $c_1 = 123/16$  and  $c_2 = 145/112$ ,  $p_1 = \sqrt{3}c_1^2/[1 + 3(\delta - 2\gamma)^2]$  ( $> 0$ ) and  $p_2 = c_1^2(3\delta - 6\gamma)/[1 + 3(\delta - 2\gamma)^2]$ .

From eqs.(28) and (29), we obtain the following expansion of the non-zero solutions with respect to  $\beta - \beta_c$ :

$$A = \left[ \frac{\beta_c}{c_2 \delta} (\beta_c - \beta) \right]^{1/2} \exp(i\theta) + O(|\beta - \beta_c|^{3/2}) \text{ for } \delta \neq 0, \quad (30)$$

$$A = \left[ \frac{2}{2p_1 + c_2^2} (\beta - 1) \right]^{1/4} \exp\left(i\frac{\pi}{4}\right) + O(|\beta - 1|^{5/4}) \text{ for } \delta = 0, \quad (31)$$

where  $\exp(i\theta) = [(\beta_c + \delta)/(2\beta_c)]^{1/2} + i[(\beta_c - \delta)/(2\beta_c)]^{1/2}$ . In eqs.(30) and (31),  $\delta(\beta_c - \beta)$  and  $\beta - 1$  must be positive. Therefore, the solution (30) exists for  $\beta > \beta_c$  ( $\beta < \beta_c$ ) when  $\delta < 0$  ( $\delta > 0$ ). Since the bifurcation at  $\beta = \beta_c$  is codimension 1 and the null solution is stable (unstable) when  $\beta < \beta_c$  ( $\beta > \beta_c$ ), this bifurcation is supercritical (subcritical) when  $\delta < 0$  ( $\delta > 0$ ).

## References

- [1] J. R. Wilton: *Phil. Mag. (Ser. 6)* **29** (1915) 688.

- [2] L. F. McGoldrick: *J. Fluid Mech.* **52** (1972) 725.
- [3] A. H. Nayfeh: *J. Fluid Mech.* **48** (1971) 385.
- [4] A. H. Nayfeh: *Phys. Fluids* **13** (1970) 545.
- [5] J. W. Miles: *J. Fluid Mech.* **146** (1984) 285.
- [6] J. W. Miles: *Proc. R. Soc. London, Ser. A* **297** (1967) 459.
- [7] S. P. Decent: *Fluid Dyn. Res.* **19** (1997) 201.